Post-irradiation examination of low burnup U_3Si_5 and UN-U_3Si_5 composite fuels

William A. Hanson[1], Fabiola. Cappia[1,*], Joshua T. White[2], Kenneth J. McClellan[2], Jason M. Harp[1,3]

1. *Idaho National Laboratory, Characterization and Advanced Post Irradiation Examination Division, P. O. Box 1625, Idaho Falls, ID 83415-6188 U.S.A.*
2. *Los Alamos National Laboratory, Materials Science and Technology Division, P.O. Box 1663, Los Alamos, NM, 87545, USA*
3. *Oak Ridge National Laboratory, Reactor and Nuclear Systems Division, P.O. Box 2008, Oak Ridge, TN, 37831, USA*

*Corresponding Author: fabiola.cappia@inl.gov

Abstract

This work presents post-irradiation examination data on UN-U_3Si_5 and U_3Si_5 fuels at low burnup (i.e., < 10-15 GWd/tHM) with Kanthal AF® cladding. The results suggest good irradiation performance for both the silicide and nitride-silicide composite pellets. Optical microscopy revealed that pellet-cladding gap is still open, and limited axial cracking was observed only in UN-U_3Si_5 pellets. Microcracking was isolated to the U_3Si_5 phase in all cases and was observed in pre-irradiation and depleted pellets, indicating that it was not irradiation induced. The fission gas release was minimal for the calculated fission density achieved ($2.6 – 3.15 \times 10^{20}$ fiss/cm^3). No fission gas bubbles were observed in the optical metallography. These results suggest acceptable swelling and fission gas behavior for both the single phase and composite compositions.

1. Introduction

The 2011 Great East Japan Earthquake and Tsunami and resulting Fukushima Daiichi nuclear power plant accident catalyzed a multinational interest in the research and development of advanced nuclear fuel concepts designed for improved safety when subjected to severe accident conditions. As a result, the Department of Energy, Office of Nuclear Energy (DOE-NE) initiated the Accident Tolerant Fuels (ATF) Campaign with the goal of fostering fuel research and development. These new designs must be backwards-compatible with the existing light water reactor (LWR) fleet while improving fuel performance during nominal operations and design basis accident (DBA) and beyond design basis accident (BDBA) conditions. This improved performance is also intended to increase the lifetime of the fuel, reaching higher burnups to increase fuel and plant efficiency and reduce waste [1, 2].

An initial screening phase of the ATF campaign irradiated and characterized a broad spectrum of potential, largely unexplored, fuel and cladding candidates to provide early data on their performance under LWR conditions at contained costs. The first such irradiation campaign was the ATF-1 experiment, where several fuel and cladding concepts were subjected to power rating and temperatures, but without coolant contact, to aid in down-selecting candidates for later developmental phases [2, 3]. While all concepts share the common objective of developing an alternative fuel/cladding system with enhanced performance compared to the standard UO_2-zircaloy system, each of them focuses on different aspects. Some explored only modifications of the cladding, in an attempt to improve upon the limitations that Zr-alloys suffer during DBA and BDBA conditions, while other tests incorporated additives to UO_2 or completely changed the fuel composition, mainly to overcome the limitations of poor thermal properties of the oxide fuel. These experiments represent an extensive collaboration between national laboratories,

nuclear industry, and university partners [2]. The complete experiment test matrix is available in previous publications [4].

Among the concepts in the ATF-1 experiment, approximately half of the proposed fuel designs are comprised of uranium silicide compounds [4]. Interest in uranium silicide compunds for use as nuclear fuels is not new, with initial research dating back to 1959 [5, 6]. Current applications are focused on research and test reactor use, including a new, recently qualified low-enriched uranium (LEU) fuel [7, 8]. A potential benefit of silicide fuels is their increased thermal conductivity compared to UO_2. Moreover, the silicide's thermal conductivity increases with temperature in contrast to the oxide counterpart, offering a further benefit to thermal performance [9, 10, 11]. This is of particular interest for the ATF campaign as a potential mechanism for transferring decay heat from the fuel during a Loss of Coolant Accident (LOCA) [12]. The primary silicide compound tested is U_3Si_2, which due to its increased U-density, has an increased ^{235}U-loading without increasing the enrichment. Initial post-irradiation examination (PIE) of U_3Si_2-Zirlo rodlets showed good performance at low burnups, with limited pellet swelling and fission gas release (FGR) [3].

Previously, limited study has been conducted on the U_3Si_5 compound because it has a lower U-density and requires a higher enrichment to match the ^{235}U-loading achieved with UO_2. However, there is recent interest in U_3Si_5 as a secondary fissile phase in a composite pellet with a more U-dense compound, such as UN, increasing the overall U-loading [11, 13]. The combination with UN could also offer the advantage of an improved thermal conductivity [11, 14]. An added benefit is that sintering of UN with a U-silicide offers the advantage of lowering the temperatures necessary for densification of UN by exploiting "liquid phase sintering", as silicide compounds have a much lower melting temperature [15]. The UN-U_3Si_5 composite is of particular interest because its similar neutronic performance to UO_2, which would reduce operational changes when transitioning between the oxide and high uranium density fuel and potentially extend the cycle life through increased ^{235}U-loading [11, 16, 13]. Until the ATF-1 irradiation experiment, this fuel form was purely theoretical, and little un-irradiated data of either U_3Si_5 or UN-U_3Si_5 was available before the compositions were selected for this campaign by Los Alamos National Laboratory (LANL) [11, 17]. Prior to this experiment only a single, very low dose (0.02 dpa) neutron irradiation test was conducted on U_3Si_5 [18]. The irradiation performance of UN was characterized historically to high burnup and was demonstrated to have good phase and dimensional stability with minimal fission gas release [19, 20, 21]. More recently, PIE was completed for solid solution U(N,C) MiniFuel kernels which showed limited fission product release and swelling; however, this test was only to a low burnup [22]. Additionally, irradiations continue investigating mixed nitride (U,Pu)N fuel [23]. The PIE presented in this work represents the first evaluation of the irradiation performance of both the composite fuel concept and U_3Si_5 pellets to low burnup. Additionally, most studies for nitride fuels have focused predominantly on fast reactor application conditions, so the LWR conditions targeted for this work for the composite fuel with a high UN vol% will provide valuable data for the thermal neutron performance of UN.

2. Materials and Methods

2.1 Experiment Test Matrix

As the primary goal of the ATF-1 campaign is to screen fuel concepts prior to full-size test insertions within a test or commercial reactor coolant loop, an ATR drop-in style experiment was designed to fully contain the experimental rodlets, which mimic a small section of a Pressurized Water Reactor (PWR) fuel

pin, within stainless steel capsules that isolate them from the reactor primary coolant. The details of this drop-in experiment design have been described thoroughly in the literature and will not be repeated here [24, 3]. The subjects of this work are three rodlets fabricated by LANL, two of which contain UN-U_3Si_5 composite fuel pellets and one of which contains U_3Si_5 pellets. This third rodlet was irradiated to provide baseline data on the pure silicide compound as no previous irradiation data at LWR temperature were published. All three are clad with Kanthal AF®, a commercial ferritic, Fe-Cr-Al-alloy, known for its stability and excellent oxidation resistance [25]. A summary for each rodlet is shown in Table 1.

Table 1 – Test matrix of the ATF-1 campaign rodlets fabricated at LANL

Rodlet ID	Cladding Material	Fuel Material	UN: ^{235}U Enrichment (wt%)	U_3Si_5:^{235}U Enrichment (wt%)	Average: ^{235}U Enrichment (wt%)	Predicted Burnup (GWd/tHM)
L41	Kanthal AF®	UN-U_3Si_5	4.9	8.84	5.27	10
L44	Kanthal AF®	UN-U_3Si_5	2.69	2.69	2.69	7.5
L45	Kanthal AF®	U_3Si_5	–	8.84	8.84	13.2

The enriched nitride powder was prepared using an oxide feedstock through a standard carbothermic reduction and nitridation route. U_3Si_5 was fabricated via arc melting of enriched U metal with high purity (99.999%) elemental Si weighed to stoichiometric ratios similar to the methods employed in [11]. Processing of the U_3Si_5 and UN powders and pellets was conducted in an inert Ar glove box line to minimize exposure to oxygen. Sintering was conducted in a W-mesh element furnace attached to the same glove box line. Furnace profiles for the U_3Si_5 and UN/U_3Si_5 composite material both used similar heating and cooling rates of 5 C/min, while the dwells for the U_3Si_5 were 1515 °C for 12 h and the composite at 1775 °C for 12 h.

The U_3Si_5 and UN-U_3Si_5 pellets were sintered at LANL via conventional powder metallurgical methods. For the UN-U_3Si_5 composite pellets, a target 15vol% U_3Si_5 was selected with two enrichment designs. For the L41 rodlet, the enrichment for UN was fixed at 4.9 wt% ^{235}U to match nominal LWR values. To provide a uniform ^{235}U-density across the pellets, an enrichment of 8.84 wt% ^{235}U was selected for the lower U-density U_3Si_5 phase. By contrast, a consistent 2.69 wt% ^{235}U enrichment was selected for both the UN and U_3Si_5 phases for the pellets in the L44 capsule. For the L45 capsule, the same U_3Si_5 powder that was blended into the composite L41 pellets was used to fabricate single phase pellets, 8.84 wt% ^{235}U [17].

In both the composite rodlets, L41 and L44, a stack of 9 enriched pellets was sandwiched between two depleted pellets for a total of 11 UN-U_3Si_5 pellets within the rodlets. In rodlet L45, a stack of 8 enriched U_3Si_5 pellets was sandwiched between two depleted UN-U_3Si_5 pellets. It should be noted that since fuel swelling behavior of these compounds was unknown, a conservative approach was taken, and the rodlets were fabricated with a gap greater than is used in standard PWR rods. The full details on the fabrication of the fuel pellets and experiment rodlets and their pre-irradiation characterization have been released elsewhere [17].

2.2 Irradiation Conditions

A complete irradiation history of all capsules in the ATF-1 experiment has been reported previously [4]. The linear heat generation rate (LHGR) in each capsule is calculated using whole ATR core Monte Carlo (MCNP 6.0) simulations coupled with ORIGEN for depletion. The simplified ATR power history from each cycle and the initial ATR core loading are used as inputs to these simulations. The heat generation rates are then supplied to a finite element analysis code (Abaqus) to calculate the temperatures in the capsule. The axial variation in power is minimal, and temperature is only 10-20°C; therefore, only maximum centerline temperatures are reported here. The Linear Heat Generation Rate (LHGR), fuel centerline temperature, and peak inner cladding temperature (PICT) simplified histories are recorded in Figure 1. It should be noted that the L44 rodlet was inserted in a later cycle than L41 and L45, which is the reason for the shift in cycles relative to the equivalent full power days (EFPD) [4]. The higher initial enrichments of rodlets L41 and L45, 5.27 and 8.84 wt% ^{235}U, respectively, are clearly reflected in each of the subplots in Figure 1, with a respective 26% and 27% increase in the average LHGR in subplot (a), as compared to the lower enriched L44 rodlet, 2.69 wt% ^{235}U.

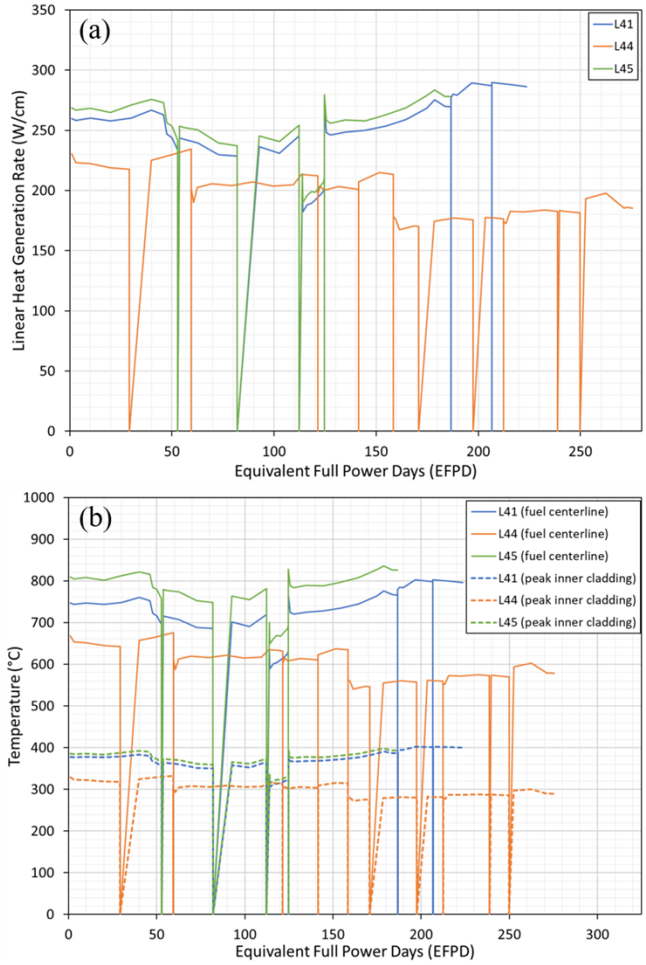

Figure 1 – Irradiation history data for L41, L44 and L45. (a) Linear Heat Generation Rate (LHGR), (b) Fuel centerline and cladding inner peak temperatures

2.3 Post-irradiation Examination Techniques

Post-irradiation examination was conducted at the INL Materials and Fuels Complex (MFC) Hot Fuels Examination Facility (HFEF). Non-destructive examination (NDE) PIE of the irradiation capsules was reported in detail previously [24, 26, 27]. In summary, visual examinations, neutron radiography, and axial resolved gamma spectrometry were performed on the irradiated capsules before capsule disassembly.

After these analyses confirmed the rodlets appeared intact, the capsules were disassembled, and the standard suite of rodlet NDE PIE was performed, consistent with the PIE performed in previous ATF-1 experiments. The methods for these characterizations have been discussed in depth previously and will only be summarized here [3]. Visual examination of the rodlets were performed through the HFEF main-cell windows. Indirect neutron radiography, using both thermal and epithermal energies, was performed using the HFEF NRAD reactor [28]. Dimensional inspections were performed on each rodlet using the BONA4INL measurement bench which utilizes opposing Sony Magnascale probes to measure diameter changes in axial scans with a 3 μm diameter resolution and 20 μm axial accuracy, and a 0.1° rotational accuracy. A total of 36 scans with measurements captured every 0.5 mm were performed in 5° increments about each rodlet. Gamma spectrometry was performed using the HFEF Precision Gamma Scanner (PGS) [29], to gather both axial scans of the individual rodlets and rotational scans at several angles for 2D tomographic reconstruction [3, 29, 30].

Following the NDE PIE, destructive examinations (DE) were performed on the rodlets, consistent with the methodologies used and detailed previously in earlier ATF-1 PIE characterizations [3]. In summary, first a fission gas analysis was performed on the plenum gas, using the HFEF Gas Assay, Sample, and Recharge (GASR) system. The rodlets were punctured using a 150 W Nd-YAG laser system, and the gas was sampled for gas mass spectrometry analysis at Pacific Northwest National Laboratory (PNNL). Pressures were monitored during the initial puncture and during a series of controlled He backfill volume expansions, through the GASR system, to arrive at the initial plenum gas pressure at puncture. Ultimately the fission gas release was determined through this pressure and the gas compositional analysis [26, 3, 29]. The rodlets were then sectioned radially to produce cross-sections of the rodlets at multiple axial heights, which were mounted in epoxy and polished for microstructural analysis and cladding microhardness analysis.

3. Results

3.1 Non-destructive Examination

After receipt of the capsules at HFEF, visual examinations, neutron radiography, and gamma spectrometry was performed in the as-received condition. The capsules appeared intact and neither radiography nor gamma spectrometry revealed unusual features, suggesting the integrity of the rodlets was maintained. After the external capsules were disassembled at HFEF, visual examination was performed on the ATF-1 L41, L44, and L45 rodlets. The rodlets did not present unusual features, and in all cases, the cladding surface still had a lustrous appearance, which is unsurprising given their isolation from reactor primary coolant within the capsules. Darkening was observed at the end-cap weld areas, but this has been observed and well documented in all other ATF-1 rodlets [26, 27].

3.1.1 Neutron Radiography

Neutron radiographs of all three rodlets are shown in Figure 2, The thermal regime is shown in 2a, where the enriched stack is marked by the brighter contrast, due to the contribution of the induced thermal fissions from ^{235}U. In the epithermal regime in 2b, the uppermost and the lowermost pellets appear

brighter instead. This is due to the increased neutron absorption by ^{235}U in the epithermal region and by the drop in the absorption by nitrogen compared to silicon in the composite depleted pellets at the top and bottom of the stack.

No evidence of large cracking can be seen any of the rodlets, except for a single case. The bottom enriched pellet in both the L41 and L44 UN-U_3Si_5 rodlets shows an axial crack at the outermost periphery of the pellet. Further cracking also occurred in the bottom depleted UN-U_3Si_5 pellet of the L44 rodlet, and some material has fallen at the bottom of the end cap, as indicated by the arrow in Figure 2a. The last three pellets of L41 and L44 are also slightly misaligned, suggesting that the larger gap between the pellet and cladding remains open and the pellets are free to move inside the cladding tube.

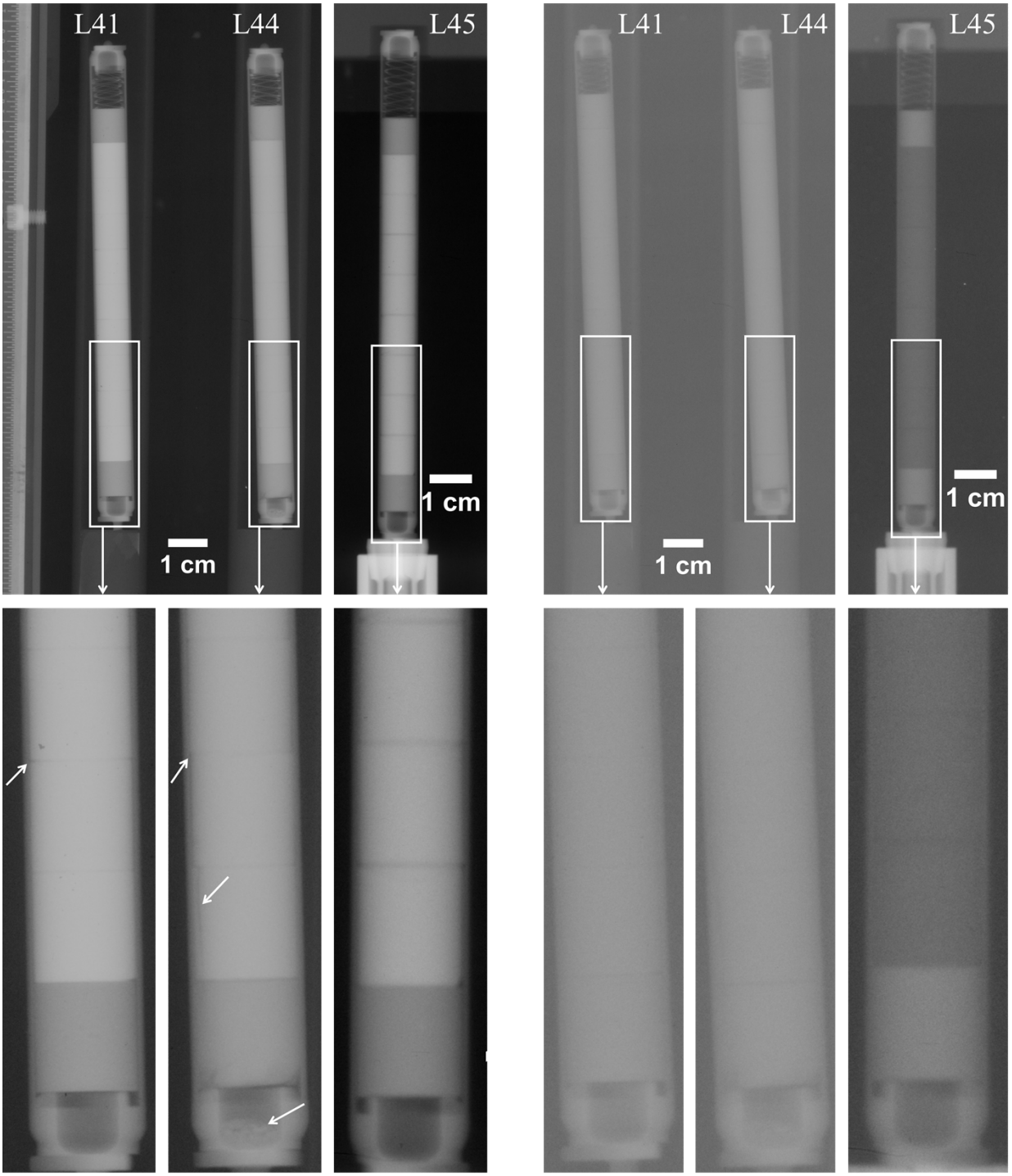

Figure 2 – Neutron radiography of the L41, L44, and L45 rodlets using (a) thermal neutrons and (b) epithermal neutrons

3.1.2 Profilometry

The angle averaged post-irradiation rodlet diameter with respect to axial position is plotted for each rodlet in Figure 3, along with the pre-irradiation mid-rodlet diameter. No significant cladding outer diameter change was measured along the entire lengths of rodlets L41 and L44, and the measured cladding outer diameter remains close to the as-fabricated nominal value, see Figure 3a and b. It should be noted that before dimensional inspection could be carried out on rodlet L45, the stub at the bottom of the rodlet, which is used to sustain the rodlet during dimensional scanning, was damaged. The measurements for this rodlet were instead conducted by inserting the rodlet directly in the measurement bench chuck. As can be seen in Figure 3c, the axial alignment of the rodlet during probe scanning is less accurate by this method and results in a measurement drift, visible through the increased uncertainty toward the rodlet ends. Despite this, at mid axial position, approximately at 50 mm in Figure 3c, the measurements appear representative, and considering fabrication uncertainties, no dimensional change was detected in this rodlet either.

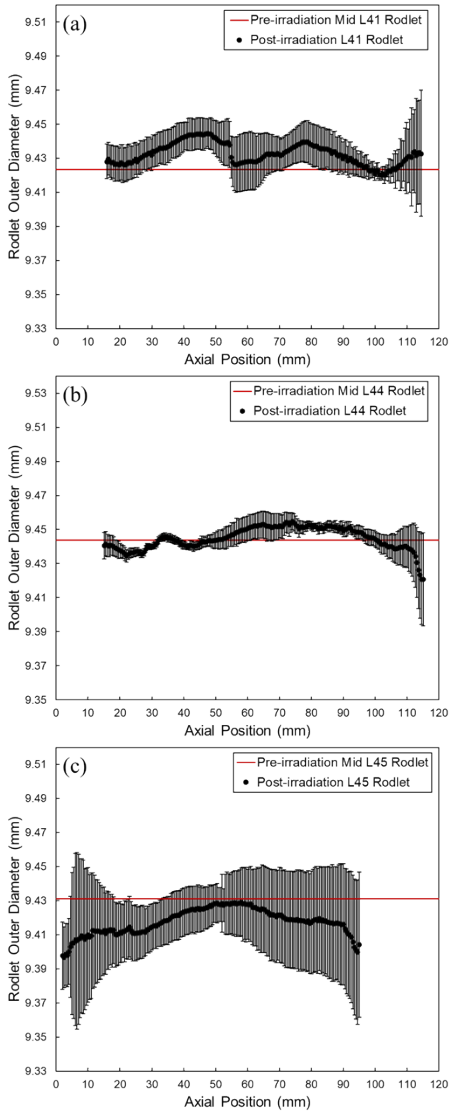

Figure 3 – Angle averaged diameter vs axial height for the (a) L41, (b) L44, and (c) L45 rodlets. The pre-irradiation mid-rodlet diameter is plotted in each case for reference.

3.1.3 Gamma Spectrometry

The axial gamma spectrometry for rodlet L45 is plotted in Figure 4 with the major fission products displayed in 4a and the primary cladding activation product shown in 4b. A clear asymmetry is observed with respect to axial position, showing an increase in both the fission and activation product profiles in the upper half of the rod. This behavior is also observed in the axial fission product profiles of the L41 and L44 rodlets, see Figure 5, suggesting a consistent behavior. This asymmetry is due to axial variation within the thermal neutron flux of the ATR core and will be discussed further below. In each case, an approximately scaled thermal neutron radiograph of the rodlet is included for reference, and enhanced signal from the fission and activation products is detected at axial positions correlating to the enriched pellets.

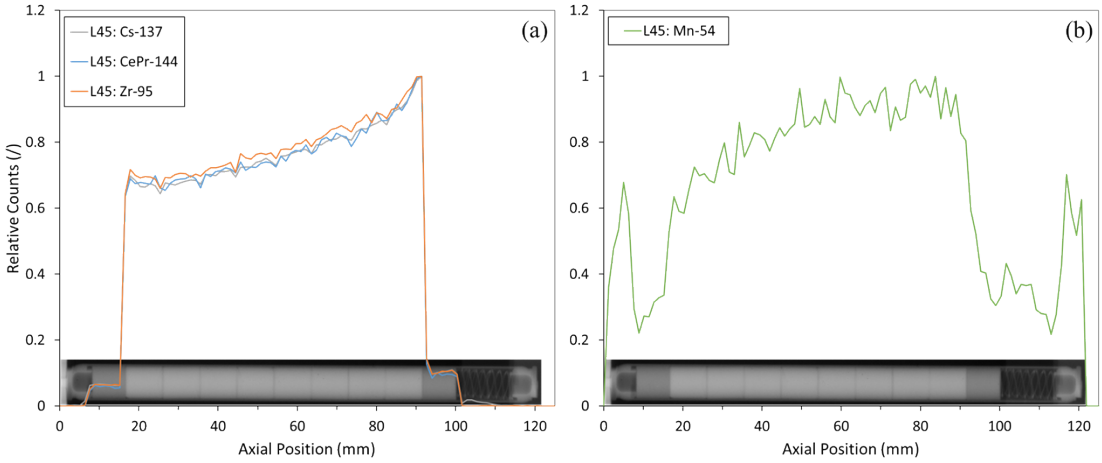

Figure 4 – Axial gamma spectra of the L45 rodlet showing (a) major fission products and (b) cladding activation product. Approximately scaled thermal neutron radiographs included for reference.

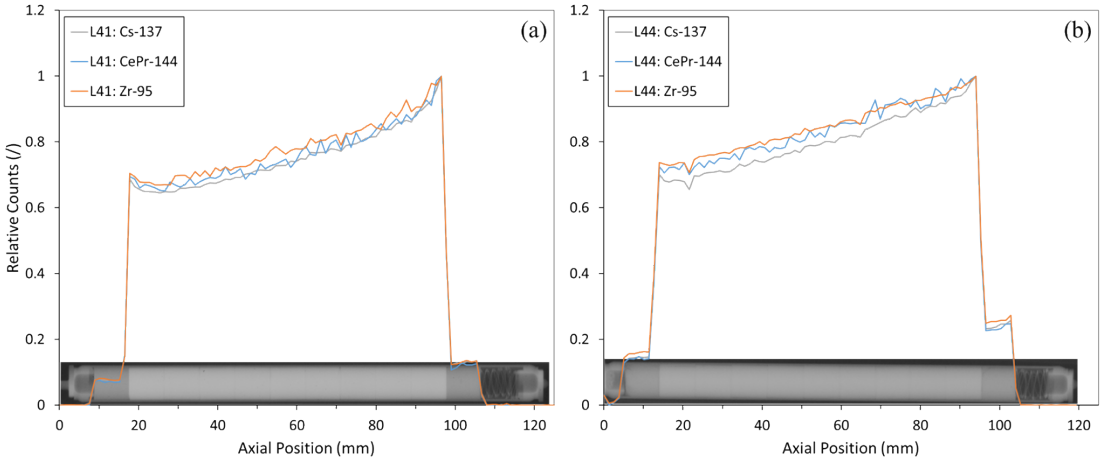

Figure 5 – Axial gamma spectra of the (a) L41 and (b) L44 rodlets showing major fission products. Approximately scaled thermal neutron radiographs included for reference.

2D tomographic reconstruction of the radial distribution of fission products are shown in Figure 6, generated from rotational gamma spectra gatherer at the center 22.2 mm of the enriched fuel stack for rodlets L45 and L44. The signals from ^{137}Cs (6a and d), ^{144}Ce-^{144}Pr (6b), and ^{95}Zr (6e), show increases along the pellet periphery, consistent with the expected increase in local burnup, due to the self-shielding effect. In L45, there is an increased signal from ^{106}Ru-^{106}Rh in the pellet center (6c) while in L44, this increase is observed in the pellet periphery (6f).

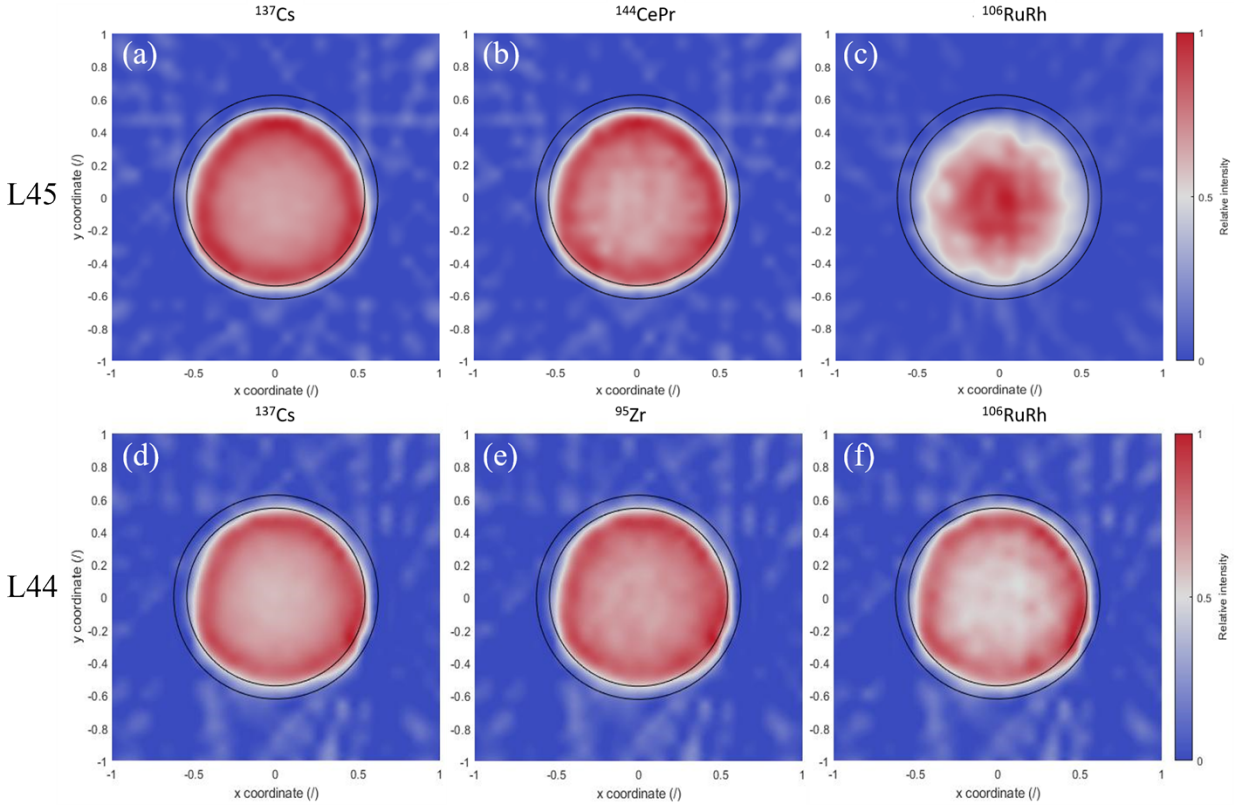

Figure 6 – Gamma tomography of selected fission products for the L45 rodlet (a-c) and the L44 rodlet (d-f)

3.2 Destructive Examination

3.2.1 Fission Gas Release and Chemical Burnup Analysis

After completion of the non-destructive examinations, the rodlets were punctured to measure the released fission gasses, and the results are summarized in Table 2**Error! Reference source not found.** for all three rodlets. The measured plenum pressure was translated into estimated fission gas release (FGR) values based on the gas inventory derived from the calculated fission densities [31]. L41 and L45 have FGR one order of magnitude higher than L44, which can be expected as the average LHGRs of L41 and L45 were 26% and 27% above that of L44, respectively, see Figure 1a.

Table 2 – Fission gas release data and calculated burnup and fission density for the three LANL rodlets

Rod ID	Calculated burnup (GWd/tHM)	Calculated fission density (fiss/cm^3)	Plenum pressure (MPa)	Plenum pressure uncertainty (%)	Estimated FGR (%)
L41	9.99	3.15E+20	0.105	7.83	0.20
L44	9.46	3.04E+20	0.102	11.03	0.01
L45	13.19	2.60E+20	0.110	6.65	0.64

3.2.2 Optical Microscopy

A radial cross section was taken from the "top" depleted UN-U_3Si_5 pellet in the L45 rodlet, and optical micrographs are shown in belowFigure 7a, and a high magnification of the composite microstructure is shown in Figure 7b. A gap is observed between the pellet and cladding in 7a, and the structure in 7b resembles the as-fabricated microstructure observed previously. The silicide phase is confined to the grain boundaries of the nitride phase, and the porosity is localized within the UN particles. Microcracking is visible within the silicide as it was in the pre-irradiated samples [17].

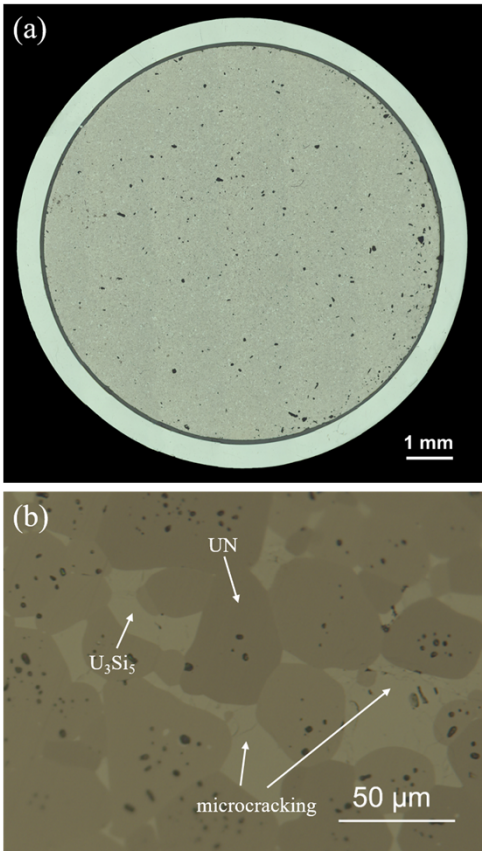

Figure 7 – Radial cross section micrographs of the UN-U_3Si_5 depleted pellet above the fuel stack of L45 at: (a) low magnification as an overview (50X) and (b) high magnification to show the structure

A radial cross-section was also taken from a U_3Si_5 pellet in the upper half of active U_3Si_5 stack (~87% stack height from the bottom), and optical micrographs are shown in Figure 8. A gap is again observed (8a) between the pellet and cladding and is more apparent in this cross-section than in the depleted pellet. No formation of fission gas bubbles could be observed on the surface, either in the center of the pellet or at the periphery (8b and c). As in the U_3Si_5 phase of the depleted sample, microcracking was observed, which was also present in the as-fabricated structure [17]. Two secondary phases were observed, with one being grey in appearance, see Figure 8b, and the other far less prevalent, lighter in color, and closer in appearance to the matrix, see previous reports for an example [26]. The phases were spread homogenously throughout the microstructure, but absent in the outer 350-400 μm of the pellet periphery, which showed a larger grain structure.

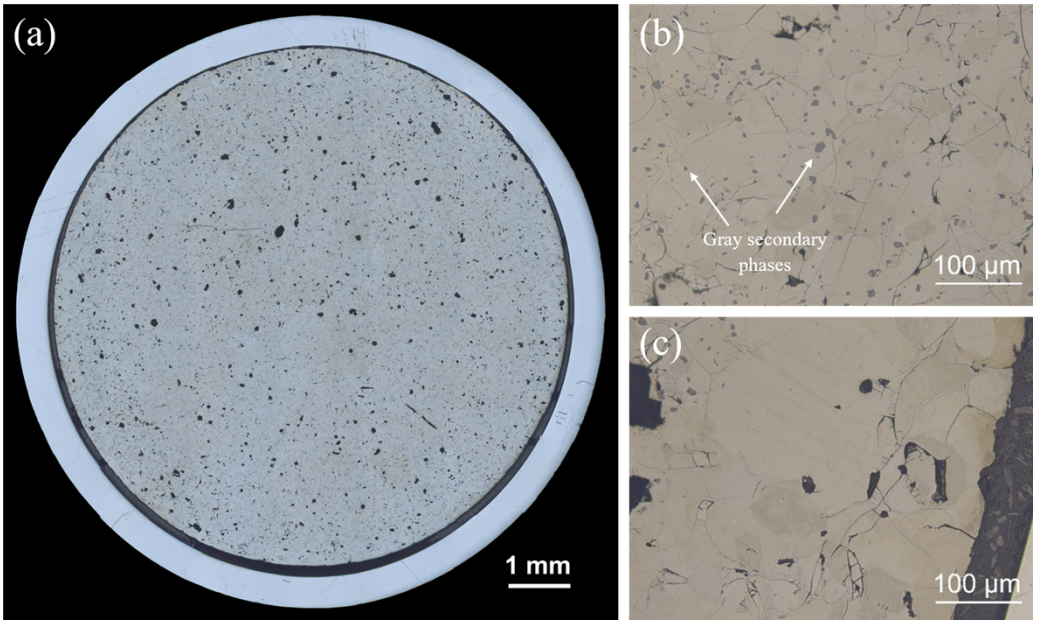

Figure 8 – Radial cross section of a U_3Si_5 pellet in the upper half of the fuel stack of L45 (87% stack height) at: (a) low magnification as an overview (50X) and high magnification to show the structure at the (b) pellet center and (c) pellet periphery

A radial cross-section was taken from the mid-axis of both the L41 and L44 rodlets, which are shown in Figure 9 and Figure 10, respectively. As in the L45 rodlet, a gap between the pellet and the cladding is observed for both rodlets (Figure 9(a) and Figure 10(a)). Each cross-section also shows some minor cracking in the pellet. Additionally, the as-fabricated microstructure appears to be retained [17], with the U_3Si_5 phase intergranular to the UN phase. Microcracks are observed predominantly within the silicide phase, but some microcracks are present in the UN phase, and porosity, again, appears localized to this nitride phase. It should be noted that brass contaminants from the microscopy sample holder are

297 embedded in the surface of the L41 and L44 mounts and are the source of the lustrous particles visible in
298 parts (b) and (c) of Figure 9 and Figure 10.

299

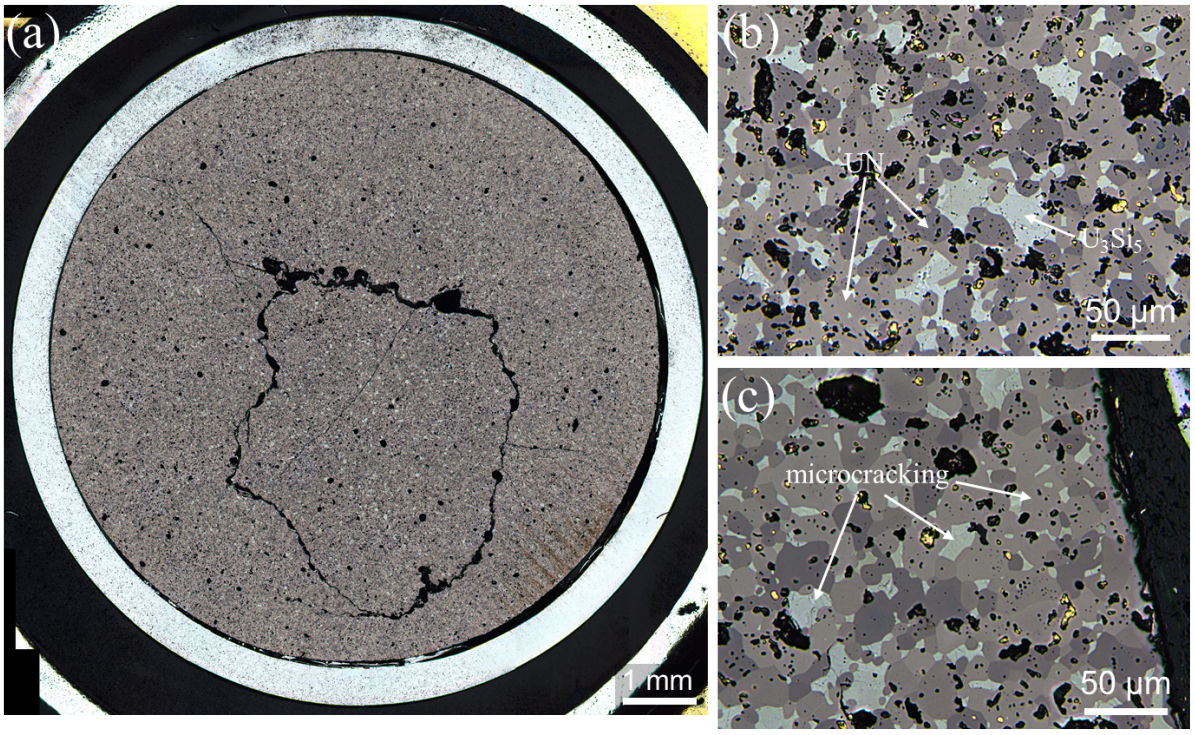

300

301 Figure 9 – Radial cross-section of a UN-U_3Si_5 pellet near the mid-axis of the L41 rodlet at: (a) low
302 magnification as an overview (50X) and high magnification to show the structure at the (b) pellet center
303 and (c) pellet periphery

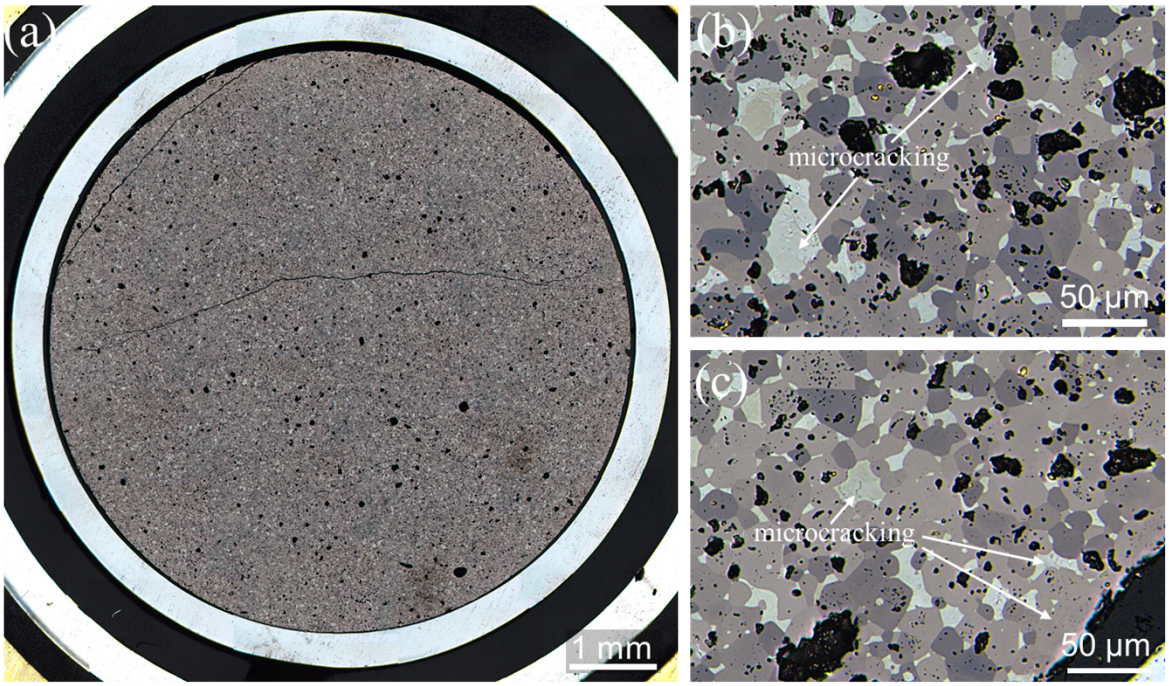

Figure 10 – Radial cross-section of a UN-U_3Si_5 pellet near the mid-axis of the L44 rodlet at: (a) low magnification as an overview (50X) and high magnification to show the structure at the (b) pellet center and (c) pellet periphery

3.2.3 Cladding Microhardness

Vickers microhardness measurements were performed across the cladding thickness every 100 μm at room temperature. The average of five measurements for each radial location on the L45 rodlet are plotted in Figure 11. Little detectable variation is observed in the hardness at each radii.

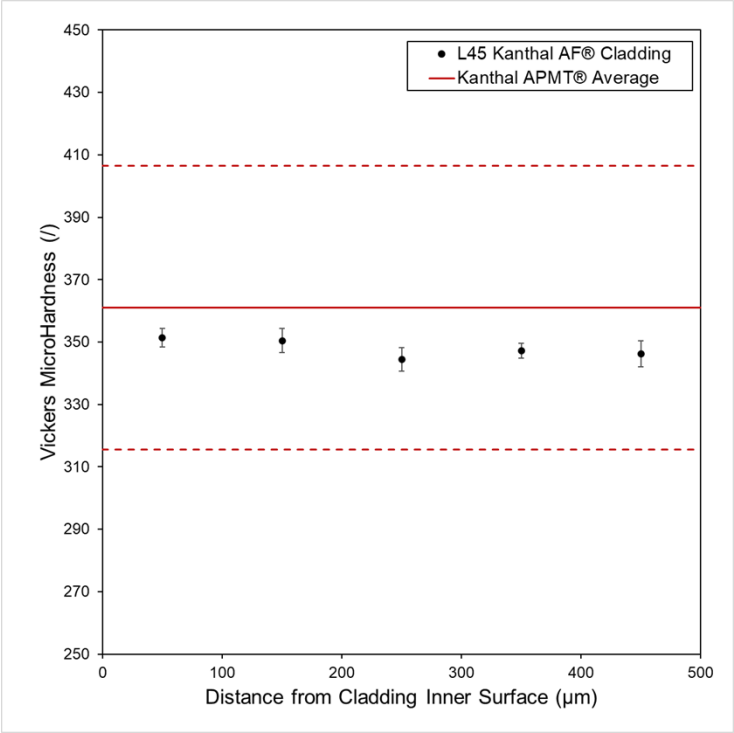

Figure 11 – Vickers microhardness profile across the cladding thickness for Kanthal AF® surrounding the fuel stack for rodlet L45. The average Vickers microhardness for unirradiated Kanthal APMT® is included for reference [32].

4. Discussion

4.1 Low Burnup Swelling and Microstructural Behavior

Part of the design of the L41, L44, and L45 rodlets was deliberate outsizing of the pellet-cladding gap within the rodlet to provide a conservative buffer as the swelling behavior of UN-U_3Si_5 was unknown. Visual inspection of the rodlets and neutron radiography did not show bulging of the cladding for any of the rodlets. A slight misalignment of the bottom pellets within L41 and L44 suggests that pellets can move freely within the cladding. This suggests that there was little contact between the pellet and cladding, which is also supported by the lack of rodlet diameter change or cladding hoop strain, ignoring the bias in the top and bottom of the L45 rodlet clarified previously. Optical microscopy confirmed these NDE analyses, revealing a clear gap between the pellets and the cladding. The porosity in the nitride phase for the enriched UN-U_3Si_5 pellets appeared consistent with the porosity of both the depleted and as-fabricated microstructure [17]. Additionally, none of the pellets showed signs of fission gas bubbles, indicating the fuel is still in a solid fission product swelling regime. Some minor axial cracks were observed in the optical microscopy of the mid-axis UN-U_3Si_5 pellets, but these were too small to be resolved with neutron radiography. The minor crack observed in L41 appears isolated to the pellet radial center and may be due to non-uniform solidification, known as “end-capping”, during the liquid phase sintering fabrication process. The only axial cracks that were resolvable with radiography were in the bottom enriched and depleted pellets from the L41 and L44 rodlets. Since these are the lowest burnup of the enriched UN-U_3Si_5 pellets and no axial cracks were observed in the optical microscopy of the L45 depleted UN-U_3Si_5 pellet, it seems likely that these minor cracks in the bottom pellets were caused during

pellets loading and by the contact with the lower end cap. In total, these results suggest that both the U_3Si_5 and UN-U_3Si_5 fuels have an acceptable swelling behavior at low burnups, approximately 15 and 10 GWd/tHM, respectively. Additional testing to higher fission densities will be necessary to confirm a stable and predictable swelling behavior.

The extensive micro-cracking, observed in both the U_3Si_5 phase of the depleted and enriched composite pellets and the U_3Si_5 pellet, was attributed to the phase transition occurring at 450°C [11] and were observed in pre-irradiation examinations as well [17]. Previous phase analyses have shown that both U-rich and UO_2 secondary phases can form in U_3Si_5 [11], which could explain the light in appearance phases observed. Further, the pre-irradiation analysis of the as-fabricated microstructure revealed the presence of UN contamination, which presented as a dark-grey phase and bears a similar shape and volume fraction to the grey phase spread through the microstructure of L45, see Figure 8. However, the isolation of the grey precipitates in the U_3Si_5 pellet to regions away from the edges could indicate that they are related to the radial redistribution of ruthenium. No previous study has been published in open literature regarding the behavior of ruthenium in U_3Si_5 that could provide a comparison with the observed microstructure. It should also be noted that the lack of ruthenium radial redistribution in the L41 and L44 pellets cannot be used to test the consistency of these observations as optical microscopy cannot distinguish between any similar precipitate phases and the primary UN phase. Energy dispersive x-ray spectroscopy analyses and other advanced PIE technique will be crucial to determine the nature of the precipitates observed.

Vickers microhardness was constant across the cladding thickness; however, Vickers microhardness measurements on un-irradiated cladding material are not available for comparison. That said, given the similar composition of Kanthal AF® to Kanthal APMT®, it can be expected that the microhardness for the previous will be similar to the latter. Indeed, hardness values are 230 and 250, respectively [25, 33]. Given this assumption, the microhardness values for the L45 rodlet Kanthal AF® cladding may be compared against those measured previously for unirradiated Kanthal APMT® [32], as plotted in Figure 11. As would be expected the L45 cladding microhardness appears slightly less than the unirradiated Kanthal APMT®. It should be noted that the slightly higher microhardness average for the L45 rodlet cladding is likely due to fabrication process as the low fast neutron flux for this experiment is unlikely to produce measurable irradiation-induced hardening.

4.2 Fission Product Behavior

Comparing axial distribution of major fission products, as measured by gamma scanning, to their respective, approximately scaled thermal neutron radiographs, a clear enhanced signal is observed to correlate with the enriched pellets of each rodlet. It is unsurprising to also see enhanced signal from the ^{54}Fe cladding activation product, ^{54}Mn, at these axial positions, due to the increased local fast fission flux. The axial distribution of each is clearly asymmetric for each rodlet, with signal increasing with axial height along the fuel stacks. However, it is unlikely that redistribution and relocation is responsible for this trend. The maximum fuel temperature observed was in the L45 rodlet and averaged ~800°C, see Figure 1b, which is low to drive Cs redistribution and axial relocation. Additionally, given the rodlets' overall length, the thermal gradient will be negligible, making a thermally-driven asymmetry even more unlikely. Rather, the asymmetry indicates there is increased burnup near the top of the rodlets. There is a known significant axial gradient in the thermal neutron flux profile at the upper and lower edges of the ATR core, and the rodlets were irradiated in the lowest position in the core. Based on neutronic calculations [31], the power at the top of the rodlet is ~120% that of the rodlet average fission power, which explains the observed gamma profile. Further evidence is seen in the secondary burnup monitors of ^{95}Zr and ^{144}Ce-^{144}Pr, which match this trend, and the trend of the ^{54}Mn cladding activation product, which suggests the fast neutron flux was higher in the top half of the rodlet.

Examining the 2D gamma tomography reconstructions, increased signals from ^{137}Cs, ^{144}Ce-^{144}Pr, and ^{95}Zr in the pellet periphery indicate an increased burnup at the edges, likely due to a self-shielding rim effect. It is interesting to note that the radial temperature gradient was sufficient in the L45 rodlet (U_3Si_5 only) to drive thermo-migration of the fission product ruthenium towards the U_3Si_5 pellet center. By contrast, this radial redistribution of Ru is not observed in the L44 pellets (U_3Si_5-UN composite). In the scanned L44 pellets, there is a sharper increase in the ^{106}Ru-^{106}Rh signal at the pellet edge than the increase seen for ^{137}Cs or ^{95}Zr. Because ^{106}Ru has a much stronger yield from ^{239}Pu fission than from ^{235}U fission this trend also indicates pellet rim Pu enrichment due to self-shielding. This enhanced rim enrichment behavior was predicted in initial model screening studies [16], and this tomography represents the first experimental evidence of the behavior in UN-U_3Si_5.

FGR remained low and fully contained. Again, the optical microscopy shows no fission gas bubbles, even in the rim regions where the burnup was higher and increased grain growth was observed in the L45 pellets. With no precipitated bubbles observed, the release must be driven by recoil events, which could partially explain the scatter observed in the low FGR% values. The centerline temperature remaining relatively low for all rodlets for the duration of the experiment likely contributed to this behavior as a similar centerline temperature for UO_2 would be well below the Vitanza threshold [34]. It should be acknowledged that while this low release behavior is consistent with other fuel systems, the GASR system does have increased uncertainty when measuring very low plenum pressures at puncture as were recorded in this experiment.

4.3 Comparison with other U-Silicides and UN-Compositions

It is appropriate to make some comparison between the U_3Si_5 and UN-U_3Si_5 fuels presented in this effort and the other U-silicide and UN-composite fuels tested to date within the ATF-1 irradiation experiment, specifically U_3Si_2. Comparing the single phases rodlets, none of the samples presented significant radial swelling as examined by NDE-PIE. Neutron radiography and optical microscopy did reveal some axial cracking in the U_3Si_2 pellets; though, this was at a significantly lower density than has been observed in UO_2 at a comparable LHGR and burnup [3]. In contrast, no cracking was observed in the U_3Si_5 pellets. A high content of Si-rich phases and UO_2 impurities were observed in the U_3Si_2 pellets while the U_3Si_5 pellets only exhibited potential UN contamination in the pellet center and less prevalent suspected U-rich phases or UO_2 impurities [3, 11]. This difference in phase purity may have played a role in the crack behavior. Gamma spectrometry revealed that neither silicide composition exhibited an axial redistribution of fission products, and a similar self-shielding was revealed in their radial distributions. The FGR was low in both cases [3].

Since the primary interest in U_3Si_5 is as a secondary fissile phase, consideration should be made of UN-U_3Si_2 composites, which could offer similar advantages to UN-U_3Si_5 composites and be fabricated using similar sintering methods but with even higher U-loading in the silicide phase [14]. To date, two such rodlets from the ATF-1 irradiation experiment have been examined for NDE–PIE. It should be unsurprising to note that the increased U-density from the primary UN phase has the same enhanced self-shielding and neutron spectrum hardening effect, and similarly results in a transuranic build-up in the pellet periphery, detected via 2D tomographic reconstructions of gamma spectra. However, unlike in the UN-U_3Si_5 pellets, radiography again revealed the presence of cracking within the pellets, perpendicular to the axial direction and attributed to loading during thermal expansion. The profilometry also showed evidence of PCMI, resulting in the permanent deformation of the cladding at the pellet-pellet interfaces, likely due to increased localized stresses from pellet hour-glassing [27]. By contrast, the UN-U_3Si_5 rodlets reported here did not show any signs of perpendicular cracking, PCMI, nor pellet hourglassing, and the axial cracking was small enough to only be resolvable with optical microscopy. While it is likely the conservative pellet-cladding gap played a role in this mechanical response [17], it should not be overlooked that the larger axial cracking observed in the single phase U_3Si_2 pellets occurred despite the pellet-cladding gap remaining. However, it must be reiterated that this cracking in both the U_3Si_2 and UN-U_3Si_5 is significantly less than what is typical of UO_2 pellets at comparable conditions [3]. At this time, it

remains unclear if apparently higher stability and the increased oxidation resistance of the UN-U_3Si_5 composite, warrants the reducing the potential increased U-loading offered by the U_3Si_2 composites [11, 16].

5. Conclusions

Non-destructive and destructive PIE were performed on U_3Si_5 and UN-U_3Si_5 fueled rodlets from the ATF-1 irradiation experiment to assess their performance under normal LWR conditions to burnups less than 14 GWd/tHM. In general, the results suggest good irradiation performance for both the silicide and nitride-silicide composite pellets. Non-destructive examinations showed no indications of dimensional changes for the rodlets and did not detect any signs of perpendicular cracking, PCMI, nor pellet hourglassing. Subsequent transverse optical microscopy revealed that pellet-cladding gaps remained, and limited axial cracking was observed only in UN-U_3Si_5 pellets at a density significantly reduced as compared to UO_2 pellets subjected to comparable conditions. Microcracking was isolated to the U_3Si_5 phase in all cases and was observed in pre-irradiation and depleted pellets, indicating that it was not irradiation induced. Gamma tomography detected a sharp increase in the ^{106}Ru-^{106}Rh plutonium monitors in the UN-U_3Si_5 pellet periphery, which provided the first experimental evidence of rim enrichment in this composite fuel. This validated the predictions of initial composition screening models. No fission gas bubbles were observed in the optical metallography and FGR was low with no indications of loss of containment. These results suggest acceptable swelling and fission gas behavior for both the single phase and composite compositions at this burnup. Future microstructural examination with SEM and other materials science techniques will be vital for providing insight into precipitate phase compositions observed in U_3Si_5 as well as inputs to continue to validate fuel performance modeling of U_3Si_5 and UN-U_3Si_5 systems.

U.S. Department of Energy Disclaimer

Declaration of Competing Interests

The authors declare that they have no known competing interests, whether financial, personal, or relational, that could have or appeared to influence the work reported in this paper.

Credit authorship contribution statement

W. A. Hanson: Data curation, Writing – original and revised draft. **F. Cappia**: Conceptualization, Data curation, Writing – original and revised draft, **J. White**: Conceptualization, As-fabricated analysis, Writing – review and editing, **K. McClellan**: Conceptualization, As-fabricated analysis, Writing – review and editing, **J.M. Harp**: Conceptualization, Writing – review & editing.

Acknowledgements

This work is supported by the U.S. Department of Energy, under DOE Idaho Operations Office Contract DE-AC07-05ID14517 and National Nuclear Security Administration contract number 89233218CNA000001. Accordingly, the U.S. Government retains a nonexclusive, royalty-free license to publish or reproduce the published form of this contribution, or allow others to do so, for U.S. Government purposes. The authors would also like to acknowledge the staff, engineers, and operators of MFC HFEF for their efforts during the post-irradiation examinations.

6. References

[1] J. Carmack, F. Goldner, S. Bragg-Sitton and L. Snead, "Overview of the U.S. DOE Accident Tolerant Fuel Development Program," *Top Fuel 2013, INL/CON-13-29288, Idaho National Laboratory,* September 2013.

[2] S. Bragg-Sitton, M. Todosow, R. Montgomery, C. Stanek, W. Carmack and R. Montgomery, "Metrics for the technical performance evaluation of light water reactor accident-tolerant fuel," *BNL-113247-2016-JA, Brookhaven National Laboratory,* November 2016, doi:10.13182/NT15-149.

[3] F. Cappia and J. Harp, "Postirradiation examinations of low burnup U3Si2 fuel for light water reactor applications," *Journal of Nuclear Materials,* vol. 518, pp. 62-79, 2019, doi:10.1016/j.jnucmat.2019.02.047.

[4] C. Murdock, J. Brookman and C. Xing, "Accident Tolerant Fuels Series 1 (ATF-1) Irradiation Testing FY 2019 Status Report," *INL/EXT-19-55897, Idaho National Laboratory,* September 2019, doi:10.2172/1575381.

[5] A. Brown and J. Norreys, "Beta-Polymorphs of Uranium and Thorium Disilicides," *Nature,* vol. 183, p. 673, 1959, doi:10.1038/183673a0.

[6] K. Taylor and C. McMurtry, "SYNTHESIS AND FABRICATION OF REFRACTORY URANIUM COMPOUNDS. Summary Report for May 1959 through December 1960," *Metals, Ceramics, and Materials, ORO-400,* February 1961, doi:10.2172/4843747.

[7] S. VAN DEN BERGHE, A. LEENAERS, E. KOONEN and L. SANNEN, "From High to Low Enriched Uranium Fuel in Research Reactors," *Advances in Science and Technology,* vol. 73, pp. 78-90, 2010, doi:10.4028/www.scientific.net/AST.73.78.

[8] Office of Nuclear Reactor Regulation, NUREG-1313, 1988.

[9] J. White, A. Nelson, D. Byler, J. Valdez and K. McClellan, "Thermophysical properties of U3Si to 1150 K," *Journal of Nuclear Materials,* vol. 452, pp. 304-310, 2014, doi:10.1016/j.jnucmat.2014.05.037.

[10] J. White, A. Nelson, J. Dunwoody, D. Byler, D. Safarik and K. McClellan, "Thermophysical properties of U3Si2 to 1773 K," *Journal of Nuclear Materials,* vol. 464, pp. 275-280, 2015, doi: 10.1016/j.jnucmat.2015.04.031.

[11] J. White, A. Nelson, D. Byler, D. Safarik, J. Dunwoody and K. McClellan, "Thermophysical properties of U3Si5 to 1773 K," *Journal of Nuclear Materials,* vol. 456, pp. 442-448, 2015, doi:10.1016/j.jnucmat.2014.10.021.

[12] K. Terrani, D. Wang, L. Ott and R. Montgomery, "The effect of fuel thermal conductivity on the behavior of LWR cores during loss-of-coolant accidents," *Journal of Nuclear Materials,* vol. 448, p. 512–519, 2014, doi:10.1016/j.jnucmat.2013.09.051.

[13] N. Brown, M. Todosow and A. Cuadra, "Screening of advanced cladding materials and UN–U3Si5 fuel," *Journal of Nuclear Materials,* vol. 462, pp. 26-42, 2015, doi:10.1016/j.jnucmat.2015.03.016.

[14] J. White, A. Travis, J. Dunwoody and A. Nelson, "Fabrication and thermophysical property characterization of UN/U3Si2 composite fuel forms," *Journal of Nuclear Materials,* vol. 495, pp. 463-474, 2017, doi:10.1016/j.jnucmat.2017.08.041.

[15] L. Ortega, B. Blamer, J. Evans and S. McDeavitt, "Development of an accident-tolerant fuel composite from uranium mononitride (UN) and uranium sesquisilicide (U3 Si2) with increased uranium loading," *Journal of Nuclear Materials,* vol. 471, pp. 116-121, 2016, doi:10.1016/j.jnucmat.2016.01.014.

[16] N. Brown, A. Aronson, M. Todosow, R. Brito and K. McClellan, "Neutronic performance of uranium nitride composite fuels in a PWR," *Nuclear Engineering and Design,* vol. 275, pp. 393-407, 2014, doi:10.1016/j.nucengdes.2014.04.040.

[17] S. Vogel, N. Borges, A. Losko, S. Mosby, S. Voit, J. White, D. Byler, J. Dunwoody, A. Nelson and K. Mcclellan, "Neutron Characterization of Encapsulated ATF-1/LANL-1 Mockup Fuel Capsules," *LA-UR-17-28837, Los Alamos National Laboratory,* September 2017, doi:10.2172/1396105.

[18] M. Mirandou, R. González, S. Aricó and A. Fortis, "Neutron irradiation of U3Si5and Al43Mo4U6compounds. First results," *Procedia Materials Science,* vol. 9, pp. 404-411, 2015, doi:10.1016/j.mspro.2015.05.010.

[19] R. Martin, J. Gates, D. Keller, V. Storhok and W. Zielenbach, "Radiation stability of uranium mononitride," Joint U.S. - Euratome Research and Development Program, Report No. BMI-1731, UC-25 Metals, Ceramics, and Materials (TID-4500 44th Ed.), Battelle Memorial Institute, Columbus, OH, 1965.

[20] Y. Arai, "Chapter 3.02 Nitride Fuel," *Comprehensive Nuclear Materials,* vol. 3, pp. 41-54, 2012, doi:10.1016/B978-0-08-056033-5.00050-1.

[21] G. J. Youinou and R. S. Sen, "Impact of Accident-Tolerant Fuels and Claddings on the Overall Fuel Cycle: A Preliminary Systems Analysis," *Nuclear Technology,* vol. 188, no. 2, pp. 123-138, 2014, doi:10.13182/NT14-22.

[22] J. M. Harp, R. N. Morris, C. M. Petrie, J. R. Burns and K. A. Terrani, "Postirradiation examination from separate effects irradiation testing of uranium nitride kernels and coated particles," *Journal of Nuclear Materials,* vol. 544, no. 152696, 2021, doi:10.1016/j.jnucmat.2020.152696.

[23] F. Kryukov, A. Belyaeva, M. Skupov, L. Zabudko and Y. Mochalov, "Results of post-irradiation examinations of mixed nitride pins with gas and liquid metal sub-layers," *Nuclear Engineering and Design,* vol. 384, no. 111463, 2021, doi:10.1016/j.nucengdes.2021.111463.

[24] J. Harp, F. Cappia and L. Capriotti, "Postirradiation Examination of the ATF-1 Experiments - 2018 Status," *INL/EXT-18-51497, Idaho National Laboratory,* September 2018, doi:10.2172/1484529.

[25] "KANTHAL AF: Iron-Base Resistance Heating Alloy," *ASM International, Alloy Digest,* vol. 34, no. 12, ID:Fe-71, 1985, doi:10.31399/asm.ad.fe0071.

[26] F. Cappia and J. Harp, "Postirradiation Examination of the ATF-1 Experiments - 2019 Status," *INL/EXT-19-55645, Idaho National Laboratory,* September 2019.

[27] F. Cappia, "Postirradiation Examination of the ATF-1 Experiments - 2020 Status," *INL/EXT-20-59619, Idaho National Laboratory,* September 2020.

[28] A. Craft, D. Wachs, M. Okuniewski, D. Chichester, W. Williams, G. Papaioannou and A. T. Smolinski, "Neutron Radiography of Irradiated Nuclear Fuel at Idaho National Laboratory," *Physics Procedia,* vol. 69, pp. 483-490, 2015, doi:10.1016/j.phpro.2015.07.068.

[29] J. Harp, P. Demkowicz, P. Winston and J. W. Sterbentz, "An analysis of nuclear fuel burnup in the AGR-1 TRISO fuel experiment using gamma spectrometry, mass spectrometry, and computational simulation techniques," *Nuclear Engineering and Design,* vol. 278, pp. 395-405, 2014, doi:10.1016/j.nucengdes.2014.07.041.

[30] J. Harp and P. Demkowicz, "Investigation of the Feasibility of Utilizing Gamma Emission Computed Tomography in Evaluating Fission Product Migration in Irradiated TRISO Fuel Experiments," *Proceedings of the HTR 2014, INL/CON-14-31509, Idaho National Laboratory,* October 2014.

[31] B. Curnutt, J. Brookman and S. Hayes, "ATF-1 Power Histories," *TEV-3119 Rev 2, Idaho National Laboratory,* 2019.

[32] R. Rebak, P. Andresen, E. Dolley, S. Huang, Y. Kim, C. Paone, R. Stachowski, R. Fawcett, Y. Lin, K. Ledford, B. Schulz, D. Ellis, S. Maloy, A. Nelson, S. Parker, A. Parkison, G. Was, P. Ahmedabadi, B. Pint, K. Barrett, M. Teague, M. Elbakhshwan, S. Gill and L. Ecker, "Ferritic Alloys as Accident Tolerant Fuel Cladding Material for Light Water Reactors," *DE-NE0000568, Final Report Phase 1A FY2013-2014 - ATF FOA General Electric,* 2014, doi:10.2172/1166777.

[33] "KANTHAL APMT: Ferritic Resistance Alloy," *ASM International, Alloy Digest,* vol. 58, no. 6, ID:SS-1037, 2009, doi:10.31399/asm.ad.ss1037.

[34] C. Vitanza, E. Kolstad and U. Graziani, "Fission Gas Release From UO2 Pellet Fuel at High Burn-Up," in *Proceedings of American Nuclear Society topical meeting on light water reactor fuel performance*, Portland, OR, May 1979.

490

491

492

493